



# Human Ska complex and Ndc80 complex interact to form a load-bearing assembly that strengthens kinetochore–microtubule attachments

Luke A. Helgeson<sup>a</sup>, Alex Zelter<sup>a</sup>, Michael Riffle<sup>a</sup>, Michael J. MacCoss<sup>b</sup>, Charles L. Asbury<sup>c</sup>, and Trisha N. Davis<sup>a,1</sup>

<sup>a</sup>Department of Biochemistry, University of Washington, Seattle, WA 98195; <sup>b</sup>Department of Genome Sciences, University of Washington, Seattle, WA 98195; and <sup>c</sup>Department of Physiology and Biophysics, University of Washington, Seattle, WA 98195

Edited by Angelika Amon, Massachusetts Institute of Technology, Cambridge, MA, and approved February 2, 2018 (received for review October 26, 2017)

**Accurate segregation of chromosomes relies on the force-bearing capabilities of the kinetochore to robustly attach chromosomes to dynamic microtubule tips. The human Ska complex and Ndc80 complex are outer-kinetochore components that bind microtubules and are required to fully stabilize kinetochore–microtubule attachments in vivo. While purified Ska complex tracks with disassembling microtubule tips, it remains unclear whether the Ska complex–microtubule interaction is sufficiently strong to make a significant contribution to kinetochore–microtubule coupling. Alternatively, Ska complex might affect kinetochore coupling indirectly, through recruitment of phosphoregulatory factors. Using optical tweezers, we show that the Ska complex itself bears load on microtubule tips, strengthens Ndc80 complex-based tip attachments, and increases the switching dynamics of the attached microtubule tips. Cross-linking mass spectrometry suggests the Ska complex directly binds Ndc80 complex through interactions between the Ska3 unstructured C-terminal region and the coiled-coil regions of each Ndc80 complex subunit. Deletion of the Ska complex microtubule-binding domain or the Ska3 C terminus prevents Ska complex from strengthening Ndc80 complex-based attachments. Together, our results indicate that the Ska complex can directly strengthen the kinetochore–microtubule interface and regulate microtubule tip dynamics by forming an additional connection between the Ndc80 complex and the microtubule.**

kinetochore | microtubules | optical tweezers | Ska complex | Ndc80 complex

**D**epolymerizing spindle microtubules generate forces required to separate duplicated chromosomes during mitosis. The kinetochore couples dynamic microtubule ends to chromosomes and harnesses the energy released by depolymerizing microtubules to pull duplicated chromosomes to opposite poles. Kinetochore–microtubule attachments must sustain piconewton-scale loads, especially during metaphase when bioriented kinetochores are subject to tension from opposing spindle microtubules. Attachments that are too strong or too weak can generate erroneous chromosome–microtubule attachments and promote chromosome missegregation during cell division (1). The incorrect segregation of chromosomes leads to aneuploidy and has been linked to chromosomal instability (2, 3). The attachment strength established and maintained between kinetochores and dynamic microtubule ends is fundamental to faithful chromosome segregation and cell division.

In vivo experiments show that the heterotrimeric Ska complex (Ska1, Ska2, and Ska3; Fig. 1A) is important for the stability of kinetochore–microtubule coupling and suggest at least three models for how it might contribute to coupling strength. Purified Ska complex binds directly to microtubules in vitro (4), and loss of Ska complex in vivo delays mitotic progression and has been associated with chromosome congression failure and mitotic cell death (4–7). Based on these observations, one view is that the Ska complex contributes directly to kinetochore–microtubule coupling (4, 7, 8). However, some studies suggest instead that the Ska complex plays a more indirect, regulatory role in kinetochore–microtubule coupling

by recruiting protein phosphatase 1 to the kinetochore, rather than by bearing microtubule-generated forces (9). Ska complex localizes to kinetochores in vivo through interactions with the Ndc80 complex (Hec1, Nuf2, Spc24, and Spc25; Fig. 1A), an essential component of the kinetochore–microtubule interface (10–13). This observation raises a third possibility, that the Ska complex might enhance Ndc80 complex-based coupling independently of its own microtubule binding affinity (14). Purified Ska complex alone tracks with depolymerizing microtubule tips (4) and has also been found to enhance the microtubule lattice binding and tip tracking of the Ndc80 complex (15). While these findings are consistent with a direct role for Ska complex in kinetochore tip coupling, they do not address the load-bearing capacity of Ska complex-based attachments. Thus, it remains uncertain whether the Ska complex can bear significant load on microtubule ends, either alone or in combination with the Ndc80 complex.

Here, we tested the microtubule end, load-bearing strength of the human Ska and Ndc80 complexes, both together and independently. We found that Ska complex bears load at microtubule ends on its own and strengthens Ndc80 complex-based end attachments. Using cross-linking mass spectrometry, we found that the Ska3 unstructured C-terminal region of Ska complex interacts with the coiled-coil regions of the Ndc80 complex. Furthermore, we show that strengthening Ndc80 complex-based attachments requires the Ska complex to simultaneously bind the Ndc80 complex

## Significance

**Microtubules are dynamic, tube-like structures that drive the segregation of duplicated chromosomes during cell division. The Ska complex is part of a molecular machine that forms force-bearing connections between chromosomes and microtubule ends. Depletion of the Ska complex destabilizes these connections and disrupts cell division. The Ska complex binds microtubules, but it is unknown whether it directly holds force at microtubules or indirectly stabilizes the connections. Here, we show that the Ska complex makes a direct force-bearing linkage with microtubule ends and assembles with another microtubule binding component, the Ndc80 complex, to strengthen its ability to withstand force. Our results suggest that the Ska and Ndc80 complexes work together to maintain the connections between chromosomes and microtubule ends.**

Author contributions: L.A.H., C.L.A., and T.N.D. designed research; L.A.H. and A.Z. performed research; M.R., M.J.M., and C.L.A. contributed new reagents/analytic tools; L.A.H. analyzed data; and L.A.H., A.Z., C.L.A., and T.N.D. wrote the paper.

The authors declare no conflict of interest.

This article is a PNAS Direct Submission.

This open access article is distributed under [Creative Commons Attribution-NonCommercial-NoDerivatives License 4.0 \(CC BY-NC-ND\)](https://creativecommons.org/licenses/by-nc-nd/4.0/).

<sup>1</sup>To whom correspondence should be addressed. Email: [tdavis@uw.edu](mailto:tdavis@uw.edu).

This article contains supporting information online at [www.pnas.org/lookup/suppl/doi:10.1073/pnas.1718553115/-DCSupplemental](http://www.pnas.org/lookup/suppl/doi:10.1073/pnas.1718553115/-DCSupplemental).

Published online February 27, 2018.

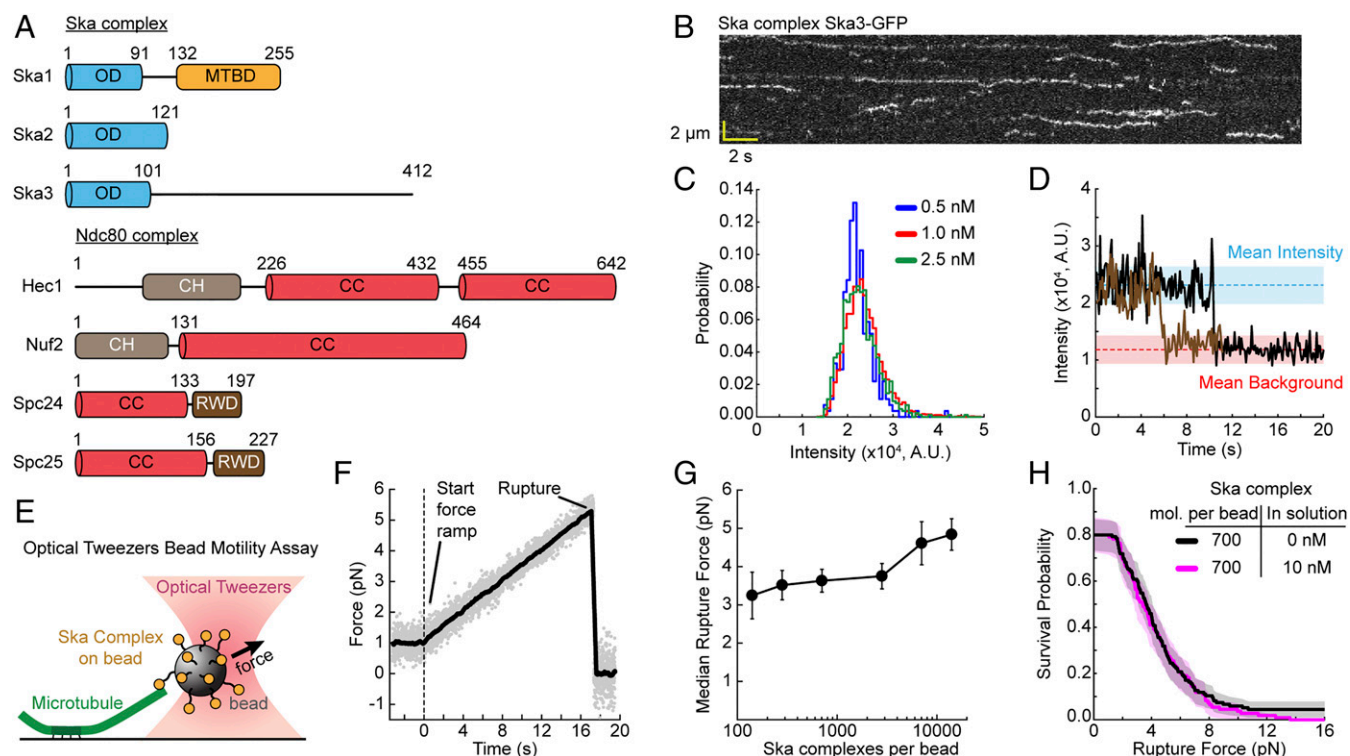


**Fig. 1.** Ska complex bears load on microtubule ends. (A) Domain architecture of the Ska complex and Ndc80 complex. CC, coiled-coil; CH, Calponin homology domain; MTBD, microtubule binding domain; OD, oligomerization domain; RWD, RING finger, WD repeat, DEAD-like helicases domain. (B) Example kymograph of Ska complex<sup>Ska3-GFP</sup> molecules binding a microtubule. (C) Histogram of tracked Ska complex<sup>Ska3-GFP</sup> particle intensities for three different concentrations. (D) Two example intensity versus time traces of tracked Ska complex<sup>Ska3-GFP</sup> particles. After loss of particle tracking, due to dissociation or bleaching, the background was sampled for several frames to calculate the background intensity. Blue dashed line indicates the mean particle intensity for all tracked molecules; red dashed line indicates the mean background intensity. Shaded regions are SD. (E) Cartoon of the optical-tweezers-based bead motility assay with Ska complex attached to the beads. A bead coated in Ska complexes is bound to the end of a dynamic microtubule. Using the optical tweezers, a force is applied that pulls on the Ska complex–microtubule connection. (F) Raw data of a Ska complex rupture force experiment (gray). Black line is data smoothed using a 50-point sliding window. Vertical dashed black line indicates start of force ramp. (G) Median rupture force versus Ska complex molecules per bead. Error bars are SD from bootstrapping analysis of the median. The median values and errors are calculated from the same data shown in Fig. S2A. (H) Rupture force survival probability plot for 700 Ska complex molecules per bead without (black) and with (magenta) 10 nM Ska complex in solution. Shaded areas are 95% confidence intervals from Kaplan–Meier analysis.

and the microtubule. Our results suggest the Ska complex and Ndc80 complex directly interact with each other and with microtubules to form a multipartite load-bearing assembly that strengthens kinetochore–microtubule attachments.

## Results

**Ska Complex Bears Load on Microtubule Ends.** The Ska complex is reported to dimerize in solution and to cooperatively bind the microtubule lattice as a dimer or as higher-order oligomers (4, 15–17). Before measuring the strength of its attachments to microtubules, we used total internal reflection fluorescence (TIRF) microscopy to examine the oligomeric state of the Ska complex at the low nanomolar concentrations used in our microtubule binding and rupture force assays. Individual particles of GFP-tagged Ska complex (Ska complex<sup>Ska3-GFP</sup>) bound and diffused along Taxol-stabilized microtubules, as reported previously, and similarly to the lattice diffusion of other kinetochore components (Fig. 1B) (15, 17–19). The mean residence time of Ska complex<sup>Ska3-GFP</sup> particles on microtubules was  $5.2 \pm 0.1$  s, similar to previously measured residence times (Fig. S1A) (15, 17). Particle intensities fell within a unimodal, approximately Gaussian distribution that did not change across a fivefold increase in concentration, and they photobleached or dissociated in single steps (Fig. 1C and D). Moreover, individual Ska complex<sup>Ska3-GFP</sup> particles, when bound sparsely onto coverslip surfaces, exhibited single-step photobleaching, and their mean intensity before bleaching

matched that of single GFP-tagged yeast Ndc80 complexes (Fig. S1B). Using size exclusion chromatography–multiangle light scattering (SEC-MALS), we confirmed that Ska complex<sup>Ska3-GFP</sup> in solution can form a dimer and exists in a monomer–dimer equilibrium at micromolar concentrations (Fig. S1C) (16). However, our TIRF data suggest that at low nanomolar concentrations, the Ska complex binds the microtubule lattice as a single complex.

Using an optical-tweezers bead motility assay, we next measured the microtubule end-binding strength of the Ska complex. We coated beads with the Ska complex at various concentrations, to control the surface density of the molecules on the bead (Fig. 1E). Depending on the surface density and molecular structure, one or more molecules can simultaneously interact with the microtubule tip, an arrangement that mimics the multivalency at kinetochore–microtubule interfaces in vivo (20, 21). Individual Ska complex-coated beads were first attached to the growing tips of single microtubules anchored to a coverslip. After an initial low force was applied and the bead was verified to track with tip growth, the force was increased gradually until the attachment ruptured (Fig. 1F). Median rupture strengths for populations of Ska complex-coated beads were 3–5 pN, depending on the surface density (Fig. 1G, Fig. S2A, and Table S1). These observations show that tip couplers based on purified Ska complex alone can bear significant loads.

Previous work shows that Ndc80 complex microtubule attachments are strengthened through avidity. Increasing the surface

density on the beads increases the number of Ndc80 complexes that can simultaneously reach the microtubule end (see below and ref. 18). To test whether the Ska complex behaves similarly, we measured the strength of Ska complex-based attachments as a function of its surface density on beads. We observed only a small, 1.5-fold increase in Ska complex attachment strength over a 100-fold range in surface density; whereas the strength of human Ndc80 complex-based attachments increased more substantially, by 4.2-fold over a 24-fold density range (Fig. 1*G*, and see Fig. 3*D*). Furthermore, addition of 10 nM free Ska complex in solution did not increase attachment strength of bead-bound Ska complex, consistent with the lack of Ska complex oligomerization at nanomolar concentrations (Fig. 1*H*). Taken together, our data show the Ska complex is load-bearing and suggest that its load-bearing capacity is largely established at low molecular surface densities and not strongly enhanced by additional Ska complexes.

**Ska Complex Ska3 C Terminus Is Not Required for Load Bearing.** To identify interacting regions between the Ska complex and microtubules, we performed cross-linking mass spectrometry of Ska complex incubated with Taxol-stabilized microtubules. In agreement with previous reports, we observed cross-links between microtubules and the Ska1 C-terminal microtubule binding domain (MTBD) as well as between microtubules and the Ska3 unstructured C terminus (residues 102–402) (Fig. 2*A* and Fig. S3) (22, 23). To test the importance of these regions for load-bearing interactions between the Ska complex and microtubules, we measured the attachment strength of mutant Ska complexes missing

either the Ska1 MTBD (Ska1  $\Delta$ MTBD) or the Ska3 C terminus (Ska3  $\Delta$ C) (Fig. 2*B*). Beads coated with mutant Ska complex<sup>Ska1  $\Delta$ MTBD</sup> failed to bind to microtubules, indicating that the MTBD is required for formation of a load-bearing attachment. In contrast, the fraction of beads coated with Ska complex<sup>Ska3  $\Delta$ C</sup> that bound microtubules was similar to wild type (Fig. 2*C*), and their end attachment strength was only slightly reduced (by 1.3-fold; Fig. 2*D* and Table S1). These observations confirm that, within the Ska complex, both Ska1 and Ska3 interact with microtubules. The Ska1 MTBD is necessary for load-bearing interactions with microtubules, whereas the Ska3 C terminus makes only a minor contribution.

**Ska Complex Strengthens Ndc80 Complex-Based Microtubule Attachments.** Ska complex increases the affinity of Ndc80 complex for the microtubule lattice and can promote Ndc80 complex tip tracking in the absence of force (15). To determine whether the Ska complex can increase the load-bearing capacity of the Ndc80 complex, we measured the rupture force of Ndc80 complex-based attachments with and without the Ska complex added free in solution (Fig. 3*A*). Adding the Ska complex strengthened Ndc80 complex-based microtubule end attachments when the Ndc80 complex was at a low surface density on the beads, but not when it was at a high density (Fig. 3*B* and *D*, Fig. S2*B*, and Table S1). The increase in strength afforded by the Ska complex at the low Ndc80 complex surface density was greater than the rupture strength of the Ska complex alone, suggesting a synergistic effect. These results show that the Ska complex strengthens Ndc80 complex-based coupling, particularly when the latter is weak due to low avidity.

Next, we tested whether the Ska complex could strengthen Ndc80 complex-based attachments that were weakened due to a decreased affinity between the Ndc80 complex and the microtubule. We introduced Aurora B phosphomimetic mutations (serine/threonine to aspartate) in all nine phosphorylation sites in the Hec1 N-terminal tail to generate the mutant, 9D Ndc80 complex. These mutations dramatically decrease the affinity of the Ndc80 complex for microtubules (19, 24, 25). As expected, we found the mutant 9D Ndc80 complex formed attachments that were significantly weaker than those formed by wild-type Ndc80 complex (Fig. 3*C*). Adding free Ska complex increased the attachment strength of the mutant 9D Ndc80 complex by more than fivefold (Fig. 3*C* and *D*). We raised the surface density of the mutant 9D Ndc80 complex on the beads by threefold and found that the Ska complex could also moderately strengthen the attachments formed at this higher density (Fig. 3*D* and Fig. S2*C*). Furthermore, we tested a mutant Ndc80 complex lacking the entire unstructured N-terminal 80-aa tail of Hec1 ( $\Delta$ N Ndc80 complex). As expected, this mutant  $\Delta$ N Ndc80 complex formed weak attachments on its own that, just like the 9D mutant, could be strengthened by the addition of free Ska complex (Fig. 3*E*). Together, these results show that the Ska complex strengthening is independent of the Hec1 N-terminal tail.

Purified yeast Ndc80 complex and native yeast kinetochore particles detach more frequently from disassembling tips than from assembling tips (18, 26). We verified that this difference also occurs for human Ndc80 complex by applying a force clamp. Beads coated with human Ndc80 complex were attached to growing tips and then subjected to a constant tension of  $\sim$ 2 pN. Under this condition, the Ndc80 complex-based couplers tracked continuously with end growth and shortening, remaining persistently attached as the tips switched spontaneously between assembling and disassembling states (Fig. 4*A* and *B*). The mean detachment rate for Ndc80 complex-based couplers from disassembling tips was 14-fold higher than from assembling tips, confirming that the coupling was less stable during tip disassembly (Fig. 4*C* and *D* and Tables S2–S6). Interestingly, adding Ska complex in solution specifically stabilized the coupling during tip disassembly, reducing the detachment rate twofold, with no apparent effect during assembly. Altogether, these results

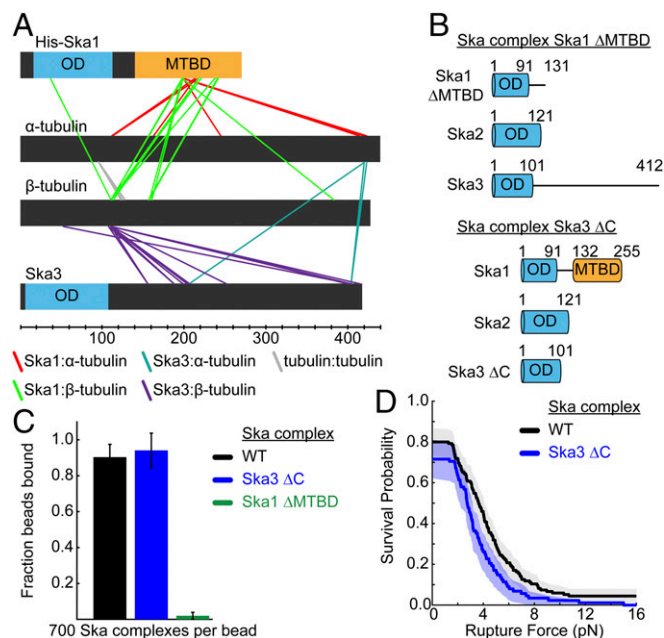


**Fig. 2.** Ska3 C terminus is not required for Ska complex load bearing on microtubule ends. (A) Cross-links identified between tubulin and Ska1 or Ska3. Cross-linking reaction with Ska complex and Taxol-stabilized microtubules was performed for 30 min with the amine-to-carboxyl cross-linker EDC. Intra-Ska complex and Ska2 cross-links are not shown for clarity; see Fig. S3 for all cross-links identified and [https://proxl.yeastrc.org/proxlv/viewProject.do?project\\_id=49](https://proxl.yeastrc.org/proxlv/viewProject.do?project_id=49) for all data. (B) Domain architecture of the Ska complex mutants. MTBD, microtubule binding domain; OD, oligomerization domain. (C) Fraction of Ska complex-coated beads that bound to microtubules: Wild-type Ska complex (black), Ska complex<sup>Ska3 $\Delta$ C</sup> (blue), Ska complex<sup>Ska1 $\Delta$ MTBD</sup> (green). Error bars are counting uncertainty. (D) Rupture force survival probability plot for 700 Ska complex molecules per bead (black) and 700 Ska complex<sup>Ska3 $\Delta$ C</sup> mutant molecules per bead (blue). Shaded areas are 95% confidence intervals from Kaplan–Meier analysis.

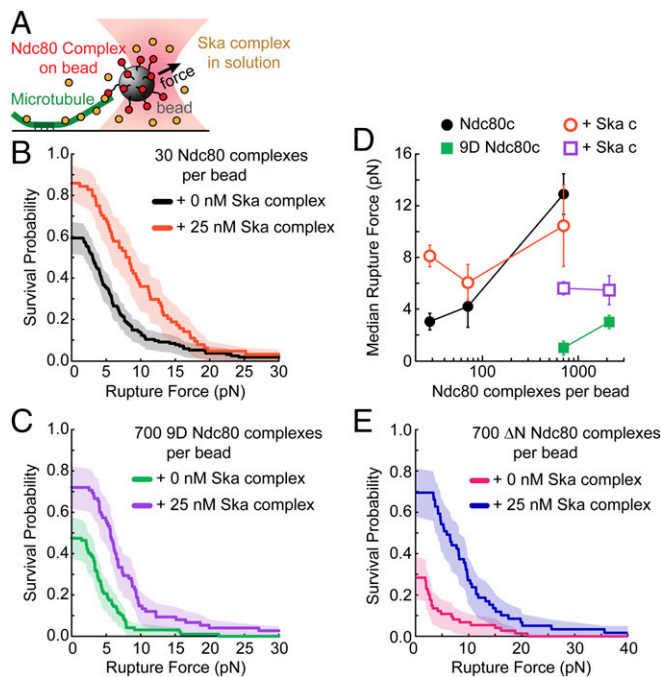


**Fig. 3.** Ska complex strengthens Ndc80 complex microtubule attachments. (A) Schematic of the optical-tweezers-based bead motility assay with Ndc80 complex attached to the bead and Ska complex free in solution. (B) Rupture force survival probability plot for 30 Ndc80 complex molecules per bead without (black) and with (orange) 25 nM Ska complex in solution. (C) Rupture force survival probability plot for 700 9D Ndc80 complex molecules per bead without (green) and with (purple) 25 nM Ska complex in solution. (D) Median rupture force versus Ndc80 complex molecules per bead. Error bars are SD from bootstrapping analysis of the median. Closed symbols are Ndc80 complex on the bead, and open symbols are Ndc80 complex on the bead with Ska complex in solution. The median values and errors are calculated from the same datasets shown in B, C, and Fig. S2 B and C. (E) Rupture force survival probability plot for 700  $\Delta$ N Ndc80 complex molecules on the bead without (magenta) or with (blue) 25 nM Ska complex in solution. All shaded regions on survival probability plots are 95% confidence intervals from Kaplan–Meier analysis.

show that Ska complex enhances Ndc80 complex-based attachment in several situations where the coupling would otherwise be relatively poor: when avidity is reduced by lowering the number of participating Ndc80 complexes, when affinity is reduced by adding phosphomimetic mutations in the Hec1 tail or removing the tail, or when attachments are intrinsically destabilized by disassembly of the microtubule tip.

**Ska Complex Changes How the Ndc80 Complex Governs Microtubule Switching Behavior.** Upon alignment at the metaphase plate, chromosomes oscillate between poleward and anti-poleward motions, which are partially driven by the switching kinetics of the kinetochore microtubules (27, 28). Altering the microtubule binding affinity of the Ska or Ndc80 complexes independently dampens these metaphase oscillations in vivo (15, 29). To test whether couplers based on the Ndc80 and Ska complexes can affect microtubule tip switching in vitro, we measured the dynamics of tips coupled to Ndc80 complex-decorated beads under a constant force, with or without Ska complex added in solution (Fig. 4 A and B and Tables S2–S6). Indeed, the rescue rate for tips attached to Ndc80 complex-based couplers increased 4.5-fold upon addition of free Ska complex (Fig. 4E). This observation is similar to previous findings showing that microtubule rescue rates increase as Ndc80 complex attachments are strengthened (19). Moreover, addition of Ska complex increased the catastrophe rate

for attached tips by 2.7-fold (Fig. 4F). These results show that the Ska complex changes how the Ndc80 complex governs microtubule behavior and suggests that together they may increase the switching frequency of kinetochore-bound microtubules.

**Ska Complex Binds the Ndc80 Complex Coiled-Coil Through the Ska3 C Terminus.** Multiple studies suggest that the Ska complex and Ndc80 complex interact directly, but the interaction interface between the complexes has not been defined (12, 13). To identify the specific regions involved in their interaction, we performed cross-linking mass spectrometry with Ska complex, Ndc80 complex, and Taxol-stabilized microtubules. The Ska3 unstructured C terminus (residues 102–412) cross-linked robustly with the Ndc80 complex and microtubules (Fig. 5A and Fig. S4). A total of 328 unique cross-links was found between the Ndc80 and Ska complexes. Of these, 97% (318 of 328) were between Ska3 and the Ndc80 complex, distributed across the Ska3 C terminus and among all four Ndc80 complex subunits. Ska3 primarily cross-linked to regions of the Ndc80 complex that are predicted to form coiled-coils. Few Ska3 cross-links were observed with the CH domains of Hec1 and Nuf2 or the RWD domains of Spc24 and Spc25. These results suggest that the Ndc80 complex and Ska complex directly interact through the Ska3 unstructured C terminus that preferentially binds to coiled-coil regions throughout the Ndc80 complex.

**The Ska Complex and Ndc80 Complex Must Bind Each Other and Microtubules to Strengthen Ndc80 Complex-Based Attachments.** The Ska complex is capable of binding directly to both the Ndc80 complex and to microtubules (4, 12, 13). We have shown that the Ska complex enhances Ndc80 complex-based coupling. Together, these observations suggest that Ska complex might form an extra

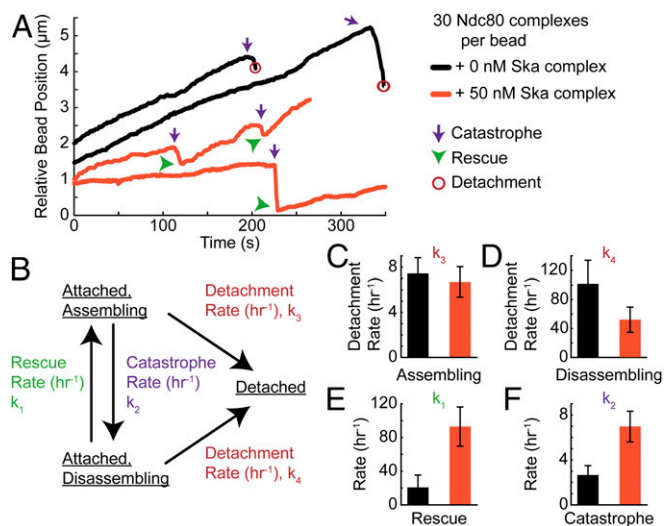


**Fig. 4.** Ska complex affects the dynamics of Ndc80 complex and bound microtubules. (A) Four example bead position versus time traces for 30 Ndc80 complex molecules per bead without (black) and with (orange) 50 nM Ska complex in solution. An average force of 2 pN was exerted on the bead. Purple arrows indicate catastrophe events; green arrowheads indicate rescue events; red open circles indicate detachment events. For clarity, the starting position of each trace is offset by an arbitrary amount. (B) Model of coupler microtubule detachment rates and microtubule switching rates measured from constant-force bead tracking experiments. (C–F) Measured rates for 30 Ndc80 complex molecules per bead without (black) and with (orange) 50 nM Ska complex in solution. Measured rates are (C) detachment rate from an assembling microtubule; (D) detachment rate from a disassembling microtubule; (E) rescue rate; and (F) catastrophe rate. Error bars are counting uncertainty.

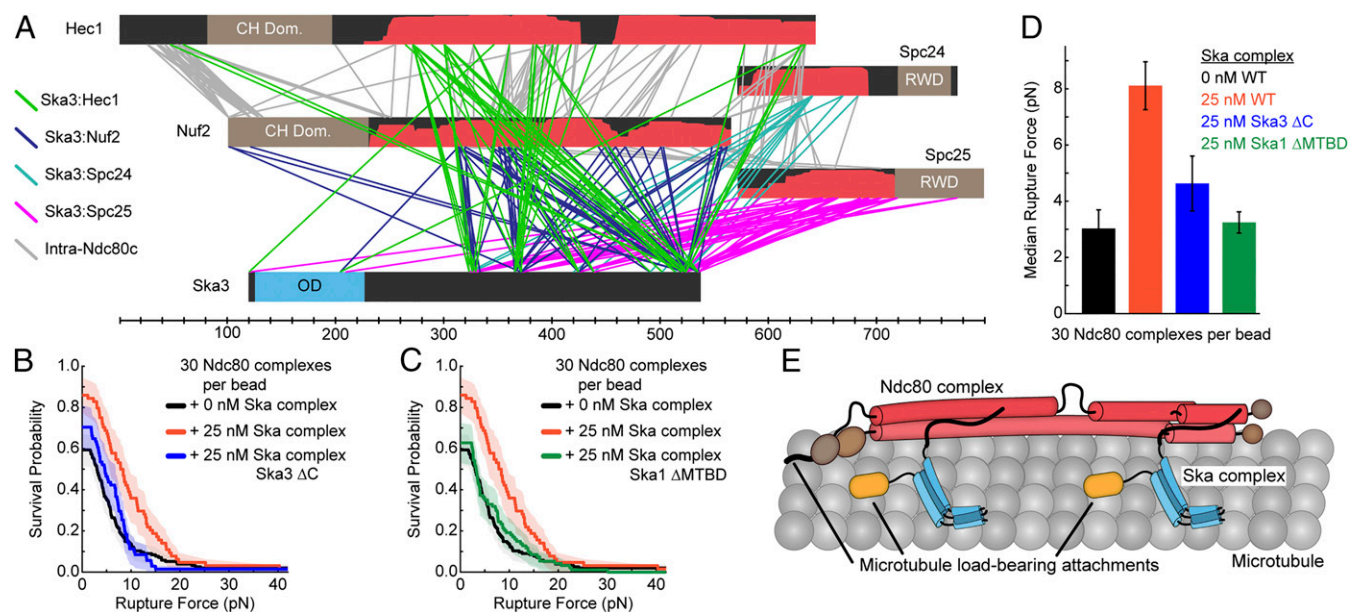


**Fig. 5.** Ska complex must bind Ndc80 complex and microtubules to strengthen attachments. (A) Cross-links identified between Ska3 and Ndc80 complex. Cross-linking reaction with Ska complex, Ndc80 complex, and Taxol-stabilized microtubules was performed for 15 min with the amine-to-amine cross-linker BS3. Ska1, Ska2, and tubulin cross-links are not shown for clarity; see Fig. S4 for all cross-links identified and [https://proxi.yeastrc.org/proxi/viewProject.do?project\\_id=49](https://proxi.yeastrc.org/proxi/viewProject.do?project_id=49) for all data. Red shaded regions indicated predicted coiled-coil (Paircoils2) with probability scores from 0.8 to 1.0. (B and C) Rupture force survival probability plot for 30 Ndc80 complex molecules per bead without Ska complex (black, data repeated from Fig. 3B) and with 25 nM Ska complex wild-type (orange, data repeated from Fig. 3B) or Ska complex<sup>Ska3  $\Delta$ C</sup> mutant (blue) or Ska complex<sup>Ska1  $\Delta$ MTBD</sup> mutant (green). All shaded regions on survival probability plots are 95% confidence intervals from Kaplan–Meier analysis. (D) Median rupture force for 30 Ndc80 complex molecules per bead with the indicated Ska complexes; colors based on B and C. WT, wild-type Ska complex. Error bars are SD from bootstrapping analysis of the median. The median values and errors are calculated from the same datasets shown in B and C. (E) Possible model of how Ska complex and Ndc80 complex directly interact to form multiple microtubule load-bearing attachments.

linkage between the Ndc80 complex and the microtubule. However, it is possible that the Ska complex-dependent enhancement of Ndc80 complex-based coupling occurs indirectly, where Ska complex affects microtubule tip structure in a way that enhances tip binding of the Ndc80 complex. To test this possibility, we measured the strength of Ndc80 complex-based tip couplers after addition of a truncated Ska complex, missing the major Ndc80 complex interaction site within the Ska3 C terminus (Ska complex<sup>Ska3  $\Delta$ C</sup>). Deletion of the Ska3 C terminus nearly abolished the ability of the Ska complex to strengthen the Ndc80 complex-based tip attachments (Fig. 5 B and D and Table S1), indicating that direct binding of the Ndc80 and Ska complexes is required for strengthening.

If the Ska complex enhances Ndc80 complex-based coupling by forming an extra linkage between the Ndc80 complex and the microtubule, then removing the major microtubule binding domain of the Ska complex should abolish the enhancement. Indeed, the mutant Ska complex<sup>Ska1  $\Delta$ MTBD</sup> was unable to strengthen Ndc80 complex attachments (Fig. 5 C and D). Cross-linking mass spectrometry with the mutant Ska complex<sup>Ska1  $\Delta$ MTBD</sup> found abundant cross-links between Ska3 and the Ndc80 complex, similar to wild type, suggesting that the mutant Ska complex<sup>Ska1  $\Delta$ MTBD</sup> retains normal interactions with the Ndc80 complex (Fig. S5). Together, these results support a model where Ska complex strengthens Ndc80 complex-based tip attachments by binding the Ndc80 complex directly and providing an additional load-bearing bridge to the microtubule (Fig. 5E).

## Discussion

Previous studies have established that depletion of the Ska complex in vivo generally weakens kinetochore–microtubule attachments, thereby (i) diminishing the numbers of attachments that are resistant to cold treatment (4, 7, 8), (ii) causing more

frequent kinetochore detachments during congression (30), and (iii) relieving the hyperstabilization of kinetochore–microtubule attachments caused by phospho-blocking mutations in the Ndc80 complex (31). Importantly, many of these weakened microtubule attachment phenotypes were also observed upon specific impairment of the microtubule-binding activity of the Ska complex. These in vivo observations are consistent with the idea that Ska complex makes a direct contribution to load bearing at the kinetochore–microtubule interface. However, the load-bearing capacity of the Ska complex has been unclear, leaving open the possibility that its role is primarily indirect, via recruitment of protein phosphatase 1 (9). We show here that the Ska complex alone can bear load on microtubule ends, that it can enhance Ndc80 complex-based coupling, and that this enhancement requires the Ska complex to bind both microtubules and Ndc80 complex. These observations strongly support the model that the Ska complex strengthens kinetochore–microtubule attachments by forming a load-bearing bridge between the Ndc80 complex and the microtubule (Fig. 5E).

Cell biological (7, 32), biochemical (15, 33), and evolutionary analyses (34) have suggested that the Ska complex might be a functional analog of the yeast Dam1 complex. However, while the Dam1 complex oligomerizes into microtubule-encircling rings that enhance its tip-coupling performance (35–37), the Ska complex does not appear to form such rings (4). Nevertheless, we find that the Ska complex, like the Dam1 complex, can form load-bearing tip attachments on its own and increase the strength and stability of Ndc80 complex-based couplers. Thus, our results lend further support to the hypothesis that the human Ska and yeast Dam1 complexes are functional analogs.

Our cross-linking mass spectrometry shows that the Ska complex interacts with the coiled-coil regions of the Ndc80 complex through the Ska3 C terminus, but the overall architecture of their

assembly at the kinetochore is unknown. Recently, the yeast Ndc80 complex was reported to bind two Dam1 complex rings and perturbations to this two-ring binding created mitotic attachment defects (38). Further structural studies will be needed to determine the assembly stoichiometry and how the Ska complex binds coiled-coil regions along the entire 55-nm-long Ndc80 complex (39). Revealing how this load-bearing unit, composed of the Ndc80 and Ska complexes, tracks with and captures the forces generated by a depolymerizing microtubule tip is critical to understanding how kinetochores translate microtubule depolymerization into chromosome segregation.

Interestingly, the enhancement of Ndc80 complex-based tip attachments upon addition of Ska complex occurred selectively, only when the Ndc80 complex-based attachments were relatively weak. We speculate that this effect might arise because Ska complex preferentially strengthens Ndc80 complex binding to a particular region on the microtubule tip, such as the most terminal tubulin subunits, and that Ndc80 complex-based couplers under weakened conditions rely primarily on bonds in this region. Alternatively, the Ska complex-dependent enhancement might be sterically blocked when Ndc80 complexes bind microtubules with high cooperativity (19, 24). While further studies will be required to understand the molecular basis for this selectivity, the effect could explain how Ska complex specifically prevents kinetochore detachments during episodes of poleward movement in prometaphase (30).

Both the Ska and Ndc80 complexes are important targets of phosphoregulation by mitotic kinases. Aurora B phosphorylates Ndc80 complex extensively during early mitosis, thereby reducing its affinity for microtubules and promoting the release of erroneous kinetochore-microtubule connections (29). During

this same period, starting in prometaphase, the Ska complex colocalizes with the Ndc80 complex (5, 13). Our finding that the Ska complex can strengthen Ndc80 complex-based microtubule attachments even when all nine Aurora B phosphorylation sites on the Ndc80 complex are mutated to phosphomimetic residues suggests that the Ska complex may partially antagonize the weakening of attachments by Aurora B during early mitosis. The Ska complex itself is also a target of the Aurora B (40), Mps1 (17), and Cdk1 (12) kinases, which are thought to regulate its interactions with microtubules and the Ndc80 complex as well as to promote its oligomerization. The ability of the Ska complex to directly strengthen kinetochore-microtubule coupling implies that selective release of erroneous attachments, and stabilization of proper bioriented attachments, may require coordinated phosphorylation of both the Ska and Ndc80 complexes.

## Materials and Methods

The human Ska and Ndc80 complexes were expressed from *Escherichia coli* cells and purified using affinity chromatography and SEC. TIRF and optical-tweezers microscopy as well as cross-linking mass spectrometry were performed as previously described (18, 38). Please see *SI Materials and Methods* for detailed descriptions of the protein purifications, TIRF microscopy, optical-tweezers microscopy, cross-linking mass spectrometry, and SEC-MALS performed in this study.

**ACKNOWLEDGMENTS.** We thank the members of the T.N.D. and C.L.A. laboratories for their helpful discussions. We thank Dr. Prasad Jallepalli for the gift of the Ska complex plasmids. This work was supported by National Institute of Health Grants F32 GM120912 (to L.A.H.), R01 GM040506 (to T.N.D.), P41 GM103533 (to M.J.M.), and R01 GM079373 (to C.L.A.), and The David and Lucile Packard Fellowship 2006-30521 (to C.L.A.).

- Cheeseman IM (2014) The kinetochore. *Cold Spring Harb Perspect Biol* 6:a015826.
- Gordon DJ, Resio B, Pellman D (2012) Causes and consequences of aneuploidy in cancer. *Nat Rev Genet* 13:189–203.
- Potapova T, Gorbisky GJ (2017) The consequences of chromosome segregation errors in mitosis and meiosis. *Biology (Basel)* 6:E12.
- Welburn JPI, et al. (2009) The human kinetochore Ska1 complex facilitates microtubule depolymerization-coupled motility. *Dev Cell* 16:374–385.
- Hanisch A, Silljé HHW, Nigg EA (2006) Timely anaphase onset requires a novel spindle and kinetochore complex comprising Ska1 and Ska2. *EMBO J* 25:5504–5515.
- Daum JR, et al. (2009) Ska3 is required for spindle checkpoint silencing and the maintenance of chromosome cohesion in mitosis. *Curr Biol* 19:1467–1472.
- Gaitanos TN, et al. (2009) Stable kinetochore-microtubule interactions depend on the Ska complex and its new component Ska3/C13Orf3. *EMBO J* 28:1442–1452.
- Raaijmakers JA, Tanenbaum ME, Maia AF, Medema RH (2009) RAMA1 is a novel kinetochore protein involved in kinetochore-microtubule attachment. *J Cell Sci* 122:2436–2445.
- Sivakumar S, et al. (2016) The human SKA complex drives the metaphase-anaphase cell cycle transition by recruiting protein phosphatase 1 to kinetochores. *eLife* 5:1–20.
- Cheeseman IM, Chappie JS, Wilson-Kubalek EM, Desai A (2006) The conserved KMN network constitutes the core microtubule-binding site of the kinetochore. *Cell* 127:983–997.
- DeLuca JG, et al. (2005) Hec1 and nuf2 are core components of the kinetochore outer plate essential for organizing microtubule attachment sites. *Mol Biol Cell* 16:519–531.
- Zhang Q, et al. (2017) Ska3 phosphorylated by Cdk1 binds Ndc80 and recruits Ska to kinetochores to promote mitotic progression. *Curr Biol* 27:1477–1484.e4.
- Janczyk PL, et al. (2017) Mechanism of Ska recruitment by Ndc80 complexes to kinetochores. *Dev Cell* 41:438–449.e4.
- Kudalkar EM, et al. (2015) Regulation of outer kinetochore Ndc80 complex-based microtubule attachments by the central kinetochore Mis12/MIND complex. *Proc Natl Acad Sci USA* 112:E5583–E5589.
- Schmidt JC, et al. (2012) The kinetochore-bound Ska1 complex tracks depolymerizing microtubules and binds to curved protofilaments. *Dev Cell* 23:968–980.
- Jeyaprakash AA, et al. (2012) Structural and functional organization of the Ska complex, a key component of the kinetochore-microtubule interface. *Mol Cell* 46:274–286.
- Maciejowski J, et al. (2017) Mps1 regulates kinetochore-microtubule attachment stability via the Ska complex to ensure error-free chromosome segregation. *Dev Cell* 41:143–156.e6.
- Powers AF, et al. (2009) The Ndc80 kinetochore complex forms load-bearing attachments to dynamic microtubule tips via biased diffusion. *Cell* 136:865–875.
- Umbreit NT, et al. (2012) The Ndc80 kinetochore complex directly modulates microtubule dynamics. *Proc Natl Acad Sci USA* 109:16113–16118.
- Dong Y, Vanden Belt DJ, Meng X, Khodjakov A, McEwen BF (2007) The outer plate in vertebrate kinetochores is a flexible network with multiple microtubule interactions. *Nat Cell Biol* 9:516–522.
- Zaytsev AV, Sundin LR, DeLuca KF, Grishchuk EL, DeLuca JG (2014) Accurate phosphoregulation of kinetochore-microtubule affinity requires unconstrained molecular interactions. *J Cell Biol* 206:45–59.
- Abad MA, et al. (2014) Structural basis for microtubule recognition by the human kinetochore Ska complex. *Nat Commun* 5:2964.
- Abad MA, et al. (2016) Ska3 ensures timely mitotic progression by interacting directly with microtubules and Ska1 microtubule binding domain. *Sci Rep* 6:34042.
- Alushin GM, et al. (2012) Multimodal microtubule binding by the Ndc80 kinetochore complex. *Nat Struct Mol Biol* 19:1161–1167.
- Zaytsev AV, et al. (2015) Multisite phosphorylation of the NDC80 complex gradually tunes its microtubule-binding affinity. *Mol Biol Cell* 26:1829–1844.
- Akiyoshi B, et al. (2010) Tension directly stabilizes reconstituted kinetochore-microtubule attachments. *Nature* 468:576–579.
- Jaqaman K, et al. (2010) Kinetochore alignment within the metaphase plate is regulated by centromere stiffness and microtubule depolymerases. *J Cell Biol* 188:665–679.
- Amaro AC, et al. (2010) Molecular control of kinetochore-microtubule dynamics and chromosome oscillations. *Nat Cell Biol* 12:319–329.
- DeLuca KF, Lens SMA, DeLuca JG (2011) Temporal changes in Hec1 phosphorylation control kinetochore-microtubule attachment stability during mitosis. *J Cell Sci* 124:622–634.
- Auckland P, Clarke NI, Royle SJ, McAinsh AD (2017) Congressing kinetochores progressively load Ska complexes to prevent force-dependent detachment. *J Cell Biol* 216:1623–1639.
- Cheerambathur DK, et al. (2017) Dephosphorylation of the Ndc80 tail stabilizes kinetochore-microtubule attachments via the Ska complex. *Dev Cell* 41:424–437.e4.
- Janke C, Ortiz J, Tanaka TU, Lechner J, Schiebel E (2002) Four new subunits of the Dam1-Duo1 complex reveal novel functions in sister kinetochore biorientation. *EMBO J* 21:181–193.
- Tien JF, et al. (2010) Cooperation of the Dam1 and Ndc80 kinetochore complexes enhances microtubule coupling and is regulated by aurora B. *J Cell Biol* 189:713–723.
- van Hooff JJE, Snel B, Kops GJPL (2017) Unique phylogenetic distributions of the Ska and Dam1 complexes support functional analogy and suggest multiple parallel displacements of Ska by Dam1. *Genome Biol Evol* 9:1295–1303.
- Westermann S, et al. (2005) Formation of a dynamic kinetochore-microtubule interface through assembly of the Dam1 ring complex. *Mol Cell* 17:277–290.
- Umbreit NT, et al. (2014) Kinetochores require oligomerization of Dam1 complex to maintain microtubule attachments against tension and promote biorientation. *Nat Commun* 5:4951.
- Asbury CL, Gestaut DR, Powers AF, Franck AD, Davis TN (2006) The Dam1 kinetochore complex harnesses microtubule dynamics to produce force and movement. *Proc Natl Acad Sci USA* 103:9873–9878.
- Kim JO, et al. (2017) The Ndc80 complex bridges two Dam1 complex rings. *eLife* 6:1–22.
- Wei RR, Sorger PK, Harrison SC (2005) Molecular organization of the Ndc80 complex, an essential kinetochore component. *Proc Natl Acad Sci USA* 102:5363–5367.
- Chan YW, Jeyaprakash AA, Nigg EA, Santamaria A (2012) Aurora B controls kinetochore-microtubule attachments by inhibiting Ska complex-KMN network interaction. *J Cell Biol* 196:563–571.

# Supporting Information

Helgeson et al. 10.1073/pnas.1718553115

## SI Materials and Methods

**Protein Expression and Purification.** Human Ska complex was generated from a dicistronic pRSF plasmid encoding Ska1 and Ska2 and a pGEX plasmid encoding GST-Ska3 (a gift from Prasad Jallepalli, Memorial Sloan Kettering Cancer Center, New York). A tobacco etch virus (TEV) protease site was introduced between the GST tag and Ska3 for affinity tag removal. All Ska complex constructs had the GST tag removed during purification. His-tagged versions of the Ska complex were generated by introducing a 6× histidine tag to the N terminus of Ska1. The amino acid sequence for Ska complex mutant constructs are as follows: Ska complex<sup>Ska3 ΔC</sup> is full-length Ska1 and Ska2 with Ska3 residues 1–101; Ska complex<sup>Ska1 ΔMTBD</sup> is full-length Ska2 and Ska3 with Ska1 residues 1–131; Ska complex<sup>Ska3-GFP</sup> is full-length Ska1 and Ska2 with GFP attached to the C terminus of full-length Ska3. Human Ndc80 complex was generated from two dicistronic plasmids encoding Hec1 and Nuf2 or Spc24-His and Spc25. GFP was attached to the C terminus of Nuf2 for *Saccharomyces cerevisiae* Ndc80 complex<sup>Nuf2-GFP</sup> (1). The 9D Ndc80 complex mutant contains the following mutations: S4D, S5D, S8D, S15D, S44D, T49D, S55D, S62D, and S69D. The ΔN Ndc80 complex mutant is residues 81–642 of Hec1 and full-length Nuf2, Spc24-His, and Spc25. Plasmids and mutations were generated using standard molecular cloning procedures and QuikChange mutagenesis (Stratagene).

Ska1, Ska2, and Ska3 were coexpressed in BL21(DE3) Rosetta 2 *E. coli* cells (Stratagene) grown for 12–16 h at 22 °C after induction with 0.3 mM isopropyl β-D-1-thiogalactopyranoside. Cells were lysed using a French Press in 50 mM sodium phosphate buffer, pH 8.0, containing the following: 300 mM NaCl, 2 mM DTT, 1 mM PMSF, 1 mM EDTA, 0.1% Tween 20, benzonase nuclease, and protease inhibitors. The lysate was clarified by a 30,000 × *g* spin for 20 min in a JA.25 rotor at 4 °C and loaded on a GS4B column (GE Life Sciences) at ~1 mL/min and 4 °C. The GS4B column was washed for three to five column volumes with 50 mM sodium phosphate buffer, pH 8.0, containing the following: 500 mM NaCl and 1 mM DTT before equilibration with a TEV cleavage buffer of 50 mM Tris buffer, pH 7.0, 150 mM NaCl, 1 mM EDTA, and 1 mM DTT. On-column TEV cleavage was performed for 12–16 h at 4 °C to cleave the GST from Ska3. The cleaved Ska complex was collected and concentrated to <2 mL using a 50,000 *M<sub>r</sub>* cutoff concentrator. Ska complex was further purified over a Superdex 200 16/60 column (GE Life Sciences) into a final buffer of 20 mM Hepes, pH 7.0, 150 mM NaCl, 5% glycerol, and 1 mM DTT, and then flash-frozen in liquid nitrogen before storage at –80 °C. Ska complex mutants were expressed and purified the same as wild type. See Fig. S6 for SDS/PAGE gels of each purified Ska complex construct. Immunoblotting was performed by first probing with a mouse anti-5×His antibody (Qiagen) followed by an IRDye 680 goat anti-mouse antibody (LI-COR). Blots were imaged using an Odyssey CLx imaging system (LI-COR).

Ndc80 complex was expressed and purified as described previously (2). In brief, Hec1, Nuf2, Spc24-His, and Spc25 were coexpressed in Rosetta 2 cells at 22 °C for 12–16 h. After lysis and clarification, Ndc80 complex was purified using Ni-NTA affinity chromatography followed by SEC using a Superdex 200 16/60 column. Ndc80 complex mutants were expressed and purified the same as wild type. Protein concentrations were determined using a bicinchoninic acid assay. See Fig. S6 for SDS/PAGE gels of purified Ndc80 complex constructs.

**TIRF Microscopy.** Ska complex microtubule binding was assessed using a custom TIRF microscope as described previously (3). Taxol-stabilized microtubules labeled at 1% with Alexa 647 were prepared by polymerizing ~20 μM tubulin at 37 °C for 30 min in the following: BRB80 (80 mM Pipes, pH 6.8, 1 mM MgCl<sub>2</sub>, 1 mM EGTA), 1 mM GTP, 6 mM MgCl<sub>2</sub>, and 3.8% DMSO. After polymerization, 10 μM Taxol was added, and microtubules were pelleted at 130,000 × *g* for 10 min at 37 °C. The microtubule pellet was resuspended in warm BRB80 with 10 μM Taxol. Flow chambers were assembled from glass slides and PEGylated coverslips as described previously (3). Flow chambers were washed with water and then incubated for 5–10 min with “rigor” kinesin in the reaction buffer: BRB80, 8 mg/mL BSA, 2 mM DTT, 40 mM glucose, 200 μg/mL glucose oxidase, and 35 μg/mL catalase. Labeled microtubules were incubated in the flow chamber for 5 min. Unbound microtubules were washed away, and then Ska complex<sup>Ska3-GFP</sup> diluted in reaction buffer was introduced into the flow chamber. The 488- and 647-nm channels were simultaneously imaged at 10 Hz for 100–200 s using an EM-CCD camera controlled with iXon software (iXon 887-BI; Andor Technology). For particles bound to the slide, Ska complex<sup>Ska3-GFP</sup> and yeast Ndc80 complex<sup>Nuf2-GFP</sup> were nonspecifically bound to the coverslip in the reaction buffer, and then free complexes were washed away. Particles bound to the slide versus bound to microtubules were measured at two different laser powers. Single-particle tracking and particle intensity analysis were performed using custom software written in Labview (National Instruments) and Matlab (Mathworks). Mean microtubule residence lifetimes and associated errors were determined by bootstrapping analysis. Kaplan–Meier analysis of survival probability curves was performed using Matlab.

**Optical Tweezers Bead Motility Assay.** Bead motility assays were performed on a custom optical tweezers microscope as described previously (4). Streptavidin-coated 0.44-μm polystyrene beads were functionalized with biotinylated anti-penta-His antibodies (Qiagen) and stored in BRB80 containing the following: 8 mg/mL BSA and 8 mM DTT. To coat beads, 14.2 pM of the anti-penta-His functionalized beads were incubated for 1 h at 4 °C with either 1–100 nM Ska complex with a His tag on the N terminus Ska1 or 0.2–15 nM Ndc80 complex with a His tag on the C terminus of Spc24. The number of molecules per bead was estimated from the molar ratios of beads to His-tagged coupler. The concentration of His-tagged couplers was calculated using BCA assays. The concentration of beads was estimated from the manufacturer’s specifications of fraction of polymer by mass in the stock solution, the polystyrene density, and the average bead diameter (Spherotech). At the concentrations tested, the beads were not saturated, based on the manufacturer’s stated biotin binding capacity per bead and on previous work showing a linear trend labeling beads with increasing concentrations of a GFP construct (1).

Microscopy flow chambers were assembled using double-sided tape, glass slides, and #1.5 coverslips. Coverslips used for Ska complex coupling experiments were plasma cleaned, whereas Ndc80 complex coupling experiments used coverslips that were acid cleaned and passivated with PEG as described previously (3). A solution of 1 mg/mL biotinylated BSA was introduced into the chamber and incubated for 15 min at room temperature, followed by a wash with BRB80; then 1 mg/mL avidin was added and incubated for 5 min before a final wash with BRB80. Biotinylated GMPCPP-stabilized microtubule seeds (0.1–0.2 mg/mL) were flown into the chamber and incubated for 5 min at room temperature before free seeds were washed away with a blocking

solution of BRB80 containing the following: 8 mg/mL BSA, 1 mM GTP, and 1 mg/mL  $\kappa$ -casein. The experiment was initiated by flowing in a solution of  $\sim 1$  pM coated beads and 5–8  $\mu$ M bovine tubulin in BRB80 containing the following: 8 mg/mL BSA, 1 mM GTP, 200  $\mu$ g/mL glucose oxidase, 35  $\mu$ g/mL catalase, 30 mM glucose, and 1 mM DTT. For in-solution Ska complex experiments, free untagged Ska complex was added to the reaction mixture at final concentrations of 10, 25, or 50 nM. The flow chamber was sealed with nail polish before data collection.

Rupture force and force-clamp experiments were performed at 26 °C on a previously described optical-tweezers instrument (4). Data were collected using in-house developed Labview software. For rupture force experiments, coated beads were bound to dynamic microtubule tips. A force of  $\sim 1$ –2 pN was applied opposite the microtubule tip, and a bead was monitored for 20–30 s to verify it was tracking with the microtubule tip. A force ramp was applied that increased the force by 0.25 pN/s until the bead ruptured from the microtubule end. For constant-force experiments, an Ndc80 complex-coated bead was bound to a dynamic microtubule tip and a constant force clamp of  $\sim 2$  pN was applied. Beads were tracked with the tip until a detachment event or the bead stuck to the coverslip. Force versus time traces were calculated using in-house routines for the Igor software package (WaveMetrics). Rupture forces, detachment events, and switching events were manually determined by examining force and position versus time traces. Survival probability curves were constructed, and medians were calculated from datasets containing beads that ruptured from microtubule ends, beads that did not hold the initial preload force of 1–2 pN, and beads that exceeded the maximum force of the instrument. Median errors were determined by bootstrapping analysis. Microtubule switching and coupler detachment rates were calculated by dividing the number of events by the total time in the assembly or disassembly state. Kaplan–Meier analysis of survival probability curves was performed using Matlab.

To confirm that the Ska complex, when added free in solution, did not bind nonspecifically to the beads, we incubated the non-His-tagged Ska complex with anti-penta-His beads in the absence of any His-tagged protein and then tested the beads for microtubule binding. Nearly all of the beads tested, 134 out of 139 (96%), failed to bind to microtubules. The few that did bind failed to hold any measurable force. Together, these results show that the Ska complex does not bind nonspecifically to the beads and they confirm that the observed strengthening of attachments (Figs. 3–5 and Fig. S2C) requires the Ska complex to bind specifically via the bead-bound Ndc80 complex.

**Cross-Linking Mass Spectrometry.** Cross-linking mass spectrometry was carried out as previously described (5, 6). For Ska complex on microtubules, a 100- $\mu$ L reaction in BRB80 was set up containing 40  $\mu$ g of Ska complex plus 10  $\mu$ g of Taxol-stabilized microtubules (made as described in *TIRF Microscopy*). Reactions were incubated for 5 min at room temperature before adding 7.5  $\mu$ L of 145 mM EDC and 3.75  $\mu$ L of 145 mM Sulfo-NHS (dissolved in BRB80). Cross-linking was performed at room temperature for 30 min before quenching by addition of 5  $\mu$ L of 1 M ammonium bicarbonate. The quenched reaction was centrifuged at 130,000  $\times$  g in a TLA100 rotor for 10 min at 37 °C, and the resulting pellet was

resuspended in 100  $\mu$ L of ice-cold PBS containing 50 mM ammonium bicarbonate plus 1  $\mu$ L of 2 M BME. The reaction was reduced for 30 min at 42 °C with 10 mM DTT and alkylated for 30 min at room temperature with 15 mM iodoacetamide. Trypsin digestion was performed at room temperature overnight with shaking at a substrate to enzyme ratio of 60:1 before acidification with 5 M HCl. For Ska complex and Ska complex<sup>Ska1  $\Delta$ MTBD</sup> plus Ndc80 complex on microtubules, 100- $\mu$ L reactions in BRB80 containing 5  $\mu$ g of Ska complex, 5  $\mu$ g of Ndc80 complex, and 5  $\mu$ g of Taxol-stabilized microtubules were set up as before. EDC reactions contained 7.5  $\mu$ L of 145 mM EDC and 3.75  $\mu$ L of 145 mM Sulfo-NHS (dissolved in BRB80) and were cross-linked for 30 min at room temperature. BS3 reactions contained 3  $\mu$ L of 14.5 mM BS3 (dissolved in BRB80) and were cross-linked for 15 min at room temperature. Quenched reactions were centrifuged as before and pellets resuspended in 50  $\mu$ L of ice-cold 20 mM ammonium bicarbonate with 0.5  $\mu$ L of 2 M BME before reduction, alkylation, and digestion as described above. Digested samples were acidified with 5 M HCl before being stored at  $-80$  °C until analysis.

Mass spectrometry and data analysis were performed on a Q-Exactive HF (Thermo Fisher Scientific) as previously described (5, 6). Sample digest (0.8–1.5  $\mu$ g) was loaded by autosampler onto a 150- $\mu$ m Kasil fritted trap packed with Reprosil-Pur C18-AQ (3- $\mu$ m bead diameter; Dr. Maisch) to a bed length of 2 cm. The trap was brought on-line with a 75- $\mu$ m i.d. Pico-Frit column (New Objective) self-packed with 30 cm of Reprosil-Pur C18-AQ (3- $\mu$ m bead diameter; Dr. Maisch). Peptides were eluted from the column at 0.25  $\mu$ L/min using a 120-min acetonitrile gradient of 2–60%. Mass spectrometry was performed on a Q-Exactive HF (Thermo Fisher Scientific) in data-dependent mode, and spectra were converted into mzML using msconvert from ProteoWizard (7). Each sample was run two to three times, and data were combined before analysis.

Cross-linked peptides were identified using Kojak, version 1.4.3 (8) (available at [www.kojak-ms.org](http://www.kojak-ms.org)). Percolator, version 2.08, was used to assign statistically meaningful  $q$  values to Kojak identifications (9). Target databases consisted of all proteins identified in the sample analyzed; decoy databases consisted of the corresponding set of reversed protein sequences. Data presented here were filtered to show hits to the target proteins that had a Percolator-assigned peptide-level  $q$  value of  $\leq 0.01$ . The complete, unfiltered list of all PSMs and their Percolator-assigned  $q$  values is available, along with the raw MS spectra and search parameters used, on the ProXL web application (10) at [https://proxl.yeastrc.org/proxl/viewProject.do?project\\_id=49](https://proxl.yeastrc.org/proxl/viewProject.do?project_id=49).

**Multiangle Light Scattering.** Size exclusion chromatography coupled with multiangle light scattering was performed on a Superdex 200 Increase 3.2/100 column (GE Life Sciences) in a buffer of 20 mM Hepes, pH 7.0, 150 mM NaCl, 5% glycerol, and 1 mM DTT. Elution from the size exclusion column was monitored by UV absorption at 280 nm, light scattering at 650 nm (miniDAWN Treos II; Wyatt Technologies), and differential refractometry (Optilab T-rEX; Wyatt Technologies). Data were analyzed using ASTRA software (Wyatt Technologies). BSA at 5 mg/mL was used to calibrate the instrument-specific parameters implemented during analysis.

1. Powers AF, et al. (2009) The Ndc80 kinetochore complex forms load-bearing attachments to dynamic microtubule tips via biased diffusion. *Cell* 136:865–875.
2. Umbreit NT, et al. (2012) The Ndc80 kinetochore complex directly modulates microtubule dynamics. *Proc Natl Acad Sci USA* 109:16113–16118.
3. Gestaut DR, et al. (2008) Phosphoregulation and depolymerization-driven movement of the Dam1 complex do not require ring formation. *Nat Cell Biol* 10:407–414.
4. Asbury CL, Gestaut DR, Powers AF, Franck AD, Davis TN (2006) The Dam1 kinetochore complex harnesses microtubule dynamics to produce force and movement. *Proc Natl Acad Sci USA* 103:9873–9878.
5. Kim JO, et al. (2017) The Ndc80 complex bridges two Dam1 complex rings. *eLife* 6:1–22.

6. Zelter A, et al. (2015) The molecular architecture of the Dam1 kinetochore complex is defined by cross-linking based structural modelling. *Nat Commun* 6:8673.
7. Chambers MC, et al. (2012) A cross-platform toolkit for mass spectrometry and proteomics. *Nat Biotechnol* 30:918–920.
8. Hoopmann MR, et al. (2015) Kojak: Efficient analysis of chemically cross-linked protein complexes. *J Proteome Res* 14:2190–2198.
9. Käll L, Canterbury JD, Weston J, Noble WS, MacCoss MJ (2007) Semi-supervised learning for peptide identification from shotgun proteomics datasets. *Nat Methods* 4:923–925.
10. Riffle M, Jaschob D, Zelter A, Davis TN (2016) ProXL (protein cross-linking database): A platform for analysis, visualization, and sharing of protein cross-linking mass spectrometry data. *J Proteome Res* 15:2863–2870.





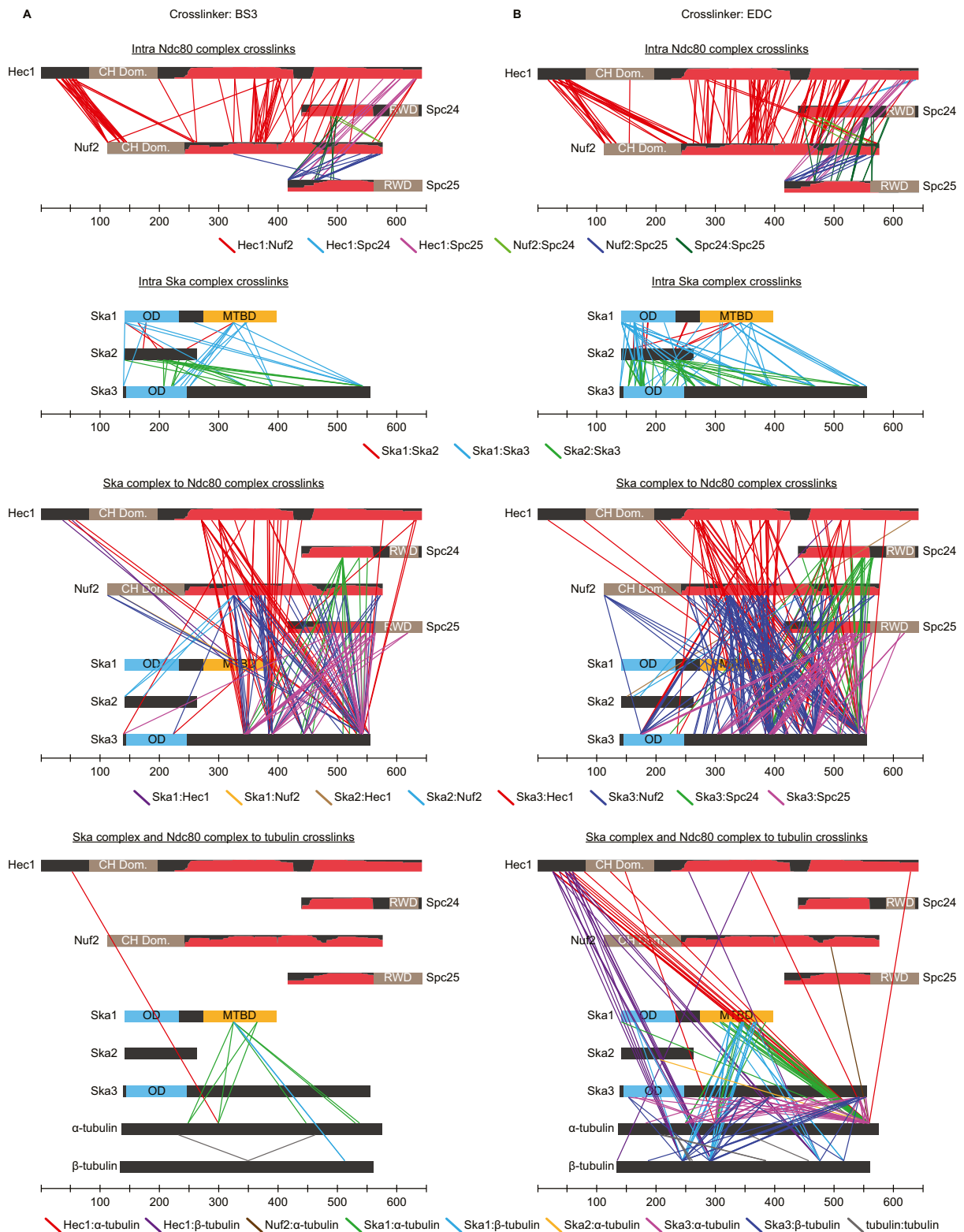


**Fig. S4.** All cross-links between Ska complex, Ndc80 complex, and microtubules. (A) All cross-links identified from the reaction with Ska complex, Ndc80 complex, and Taxol-stabilized microtubules performed for 15 min with the amine-to-amine cross-linker BS3. (B) All cross-links identified from the reaction with Ska complex, Ndc80 complex, and Taxol-stabilized microtubules performed for 30 min with the amine-to-carboxyl cross-linker EDC. All data are available at [https://proxl.yeastrc.org/proxl/viewProject.do?project\\_id=49](https://proxl.yeastrc.org/proxl/viewProject.do?project_id=49).

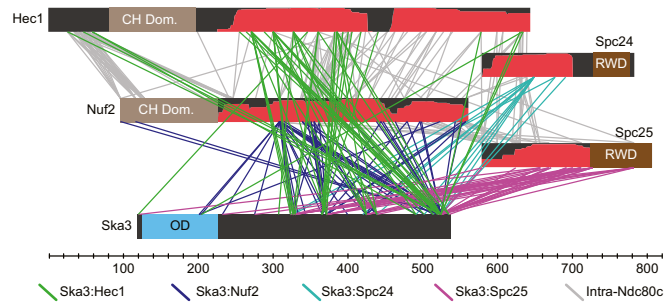


**Fig. S5.** Ska complex<sup>Ska1  $\Delta$ MTBD</sup> cross-links with Ndc80 complex through the Ska3 C terminus. Cross-links identified between Ska3 of Ska complex<sup>Ska1  $\Delta$ MTBD</sup> and Ndc80 complex. Cross-linking reaction with Ska complex<sup>Ska1  $\Delta$ MTBD</sup>, Ndc80 complex, and Taxol-stabilized microtubules was performed for 15 min with the amine-to-amine cross-linker BS3. Ska1, Ska2, and tubulin cross-links are not shown for clarity; see [https://proxl.yeastrc.org/proxl/viewProject.do?project\\_id=49](https://proxl.yeastrc.org/proxl/viewProject.do?project_id=49) for all data.

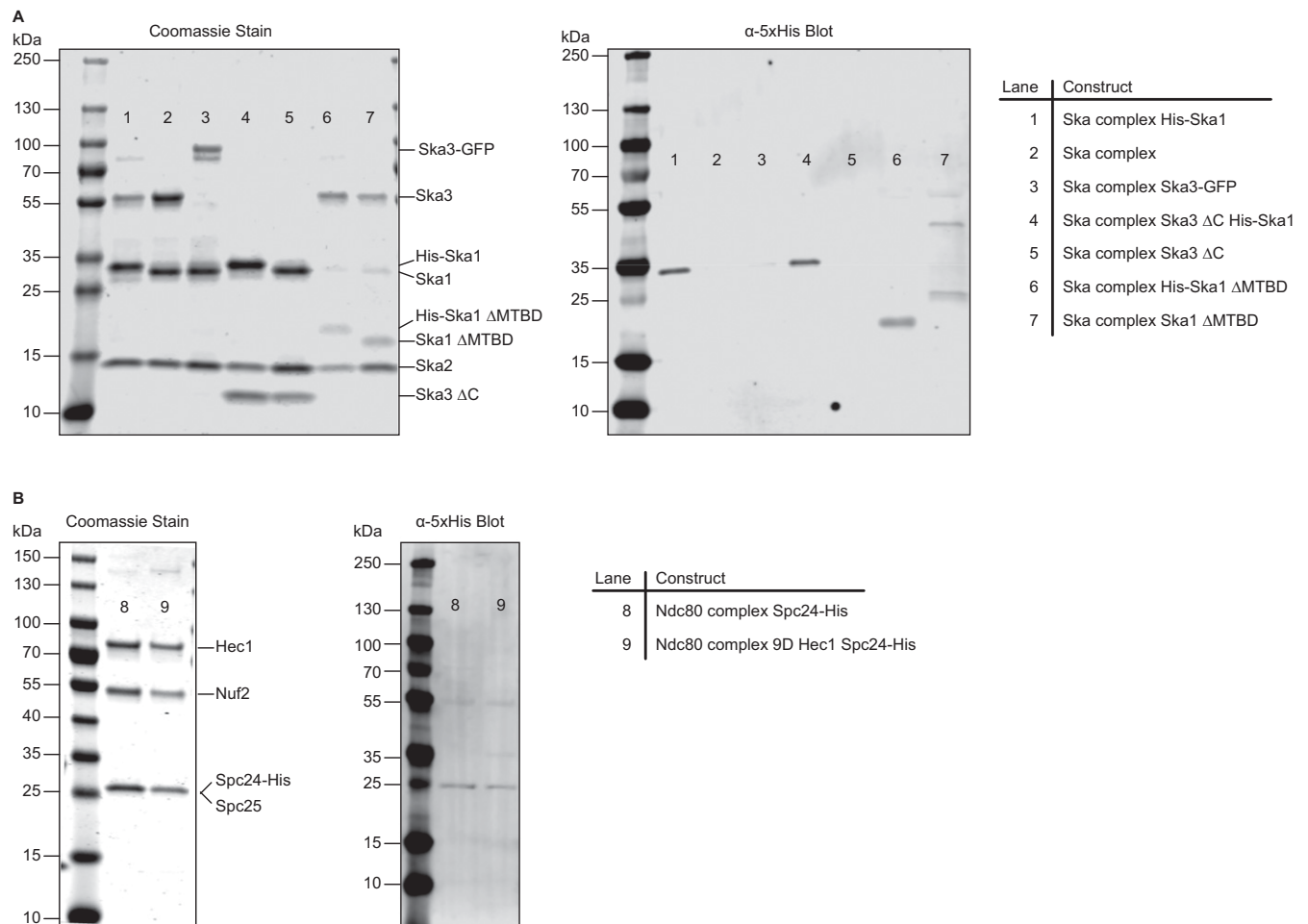


**Fig. S6.** Purified recombinant Ska and Ndc80 complexes. (A and B) SDS/PAGE gels of purified recombinant (A) Ska complexes and (B) Ndc80 complexes stained with Coomassie blue or immunoblotted with an  $\alpha$ -5xHis antibody. Samples were run on 4–20% gradient polyacrylamide gels.

**Table S1. Rupture force measurements**

Binding elements	Median rupture force, pN	Median SE, pN	N	No. beads that reached max force	No. beads that did not hold preload
<b>Ska complex alone</b>					
140 Ska complexes per bead	3.25	0.61	44	2	11
280 Ska complexes per bead	3.52	0.38	62	2	6
700 Ska complexes per bead	3.63	0.30	139	7	30
2,800 Ska complexes per bead	3.75	0.33	57	0	8
7,000 Ska complexes per bead	4.61	0.56	45	1	9
14,100 Ska complexes per bead	4.84	0.41	75	3	3
700 Ska complexes per bead + 10 nM Ska complex in solution	3.38	0.34	110	0	22
700 Ska complexes Ska1 $\Delta$ MTBD per bead	ND	ND	51	1	ND
700 Ska complexes Ska3 $\Delta$ C per bead	2.74	0.24	88	0	25
<b>Ndc80 complex and Ska complex</b>					
30 Ndc80 complexes per bead	3.03	0.64	155	3	63
70 Ndc80 complexes per bead	4.19	1.61	55	1	20
700 Ndc80 complexes per bead	12.9	1.56	66	4	8
30 Ndc80 complexes per bead + 25 nM Ska complex in solution	8.11	0.83	64	1	9
70 Ndc80 complexes per bead + 25 nM Ska complex in solution	6.05	1.40	51	1	8
700 Ndc80 complexes per bead + 25 nM Ska complex in solution	10.5	3.15	72	9	20
700 Ndc80 complexes 9D per bead	<1	0.5	97	0	51
700 Ndc80 complexes 9D per bead + 25 nM Ska complex in solution	5.61	0.51	75	1	21
2,100 Ndc80 complexes 9D per bead	3.00	0.51	86	0	34
2,100 Ndc80 complexes 9D per bead + 25 nM Ska complex in solution	5.47	1.12	70	1	14
700 Ndc80 complexes $\Delta$ N per bead	<1	ND	74	0	53
700 Ndc80 complexes $\Delta$ N per bead + 25 nM Ska complex in solution	5.88	1.22	59	1	18
30 Ndc80 complexes per bead + 25 nM Ska complex Ska3 $\Delta$ C in solution	4.63	0.99	71	21	1

ND, not determined.

**Table S2. Force clamp measurements for Ndc80 complex with and without Ska complex in solution: Catastrophe rate**

Binding elements	Total assembly time, h	No. catastrophes	Catastrophe rate, h <sup>-1</sup>	Catastrophe rate error, h <sup>-1</sup>
Ndc80 complex	3.77	10	2.65	0.84
Ndc80 complex + Ska complex	3.73	26	6.97	1.37

Error =  $\sqrt{N}/\text{time}$ .

**Table S3. Force clamp measurements for Ndc80 complex with and without Ska complex in solution: Rescue rate**

Binding elements	Total disassembly time, h	No. rescues	Rescue rate, h <sup>-1</sup>	Rescue rate error, h <sup>-1</sup>
Ndc80 complex	0.10	2	20.0	14.1
Ndc80 complex + Ska complex	0.17	16	94.1	23.5

Error =  $\sqrt{N}/\text{time}$ .

**Table S4. Force clamp measurements for Ndc80 complex with and without Ska complex in solution: Detachment rate, assembling microtubules**

Binding elements	Total assembly time, h	No. detachments	Detachment rate, h <sup>-1</sup>	Detachment rate error, h <sup>-1</sup>
Ndc80 complex	3.77	28	7.43	1.40
Ndc80 complex + Ska complex	3.73	25	6.70	1.34

Error =  $\sqrt{N}/\text{time}$ .

**Table S5. Force clamp measurements for Ndc80 complex with and without Ska complex in solution: Detachment rate, disassembling microtubules**

Binding elements	Total disassembly time, h	No. detachments	Detachment rate, h <sup>-1</sup>	Detachment rate error, h <sup>-1</sup>
Ndc80 complex	0.10	10	100	31.6
Ndc80 complex + Ska complex	0.17	9	52.9	17.6

Error =  $\sqrt{N}/\text{time}$ .

**Table S6. Force clamp measurements for Ndc80 complex with and without Ska complex in solution: Applied force**

Binding elements	No. of beads tested	No. of beads holding preload	Mean force, pN	Force SEM, pN
Ndc80 complex	192	53	1.82	0.05
Ndc80 complex + Ska complex	104	60	1.81	0.04

**Table S7. Ska complex proteins used in each experiment**

Experiments	Ska complex proteins*	Figures
<b>Optical-tweezers experiments</b>		
Rupture force with Ska complex on the bead	His-Ska1, Ska2, Ska3	Figs. 1 and 2 and Fig. S2
Rupture force with Ska complex <sup>Ska3ΔC</sup> on the bead	His-Ska1, Ska2, Ska3ΔC	Fig. 2
Rupture force with Ska complex <sup>Ska1ΔMTBD</sup> on the bead	His-Ska1ΔMTBD, Ska2, Ska3	Fig. 2
Rupture force with Ndc80 complex on the bead and Ska complex in solution	Ska1, Ska2, Ska3	Figs. 3 and 5 and Fig. S2
Force clamping with Ndc80 complex on the bead and Ska complex in solution	Ska1, Ska2, Ska3	Fig. 4
Rupture force with Ndc80 complex on the bead and Ska complex <sup>Ska3ΔC</sup> in solution	Ska1, Ska2, Ska3ΔC	Fig. 5
Rupture force with Ndc80 complex on the bead and Ska complex <sup>Ska1ΔMTBD</sup> in solution	Ska1ΔMTBD, Ska2, Ska3	Fig. 5
<b>Cross-linking experiments</b>		
Ska complex with Taxol-stabilized microtubules	His-Ska1, Ska2, Ska3	Fig. 2 and Fig. S3
Ndc80 complex with Ska complex and Taxol-stabilized microtubules	Ska1, Ska2, Ska3	Fig. 2 and Fig. S4
Ndc80 complex with Ska complex <sup>Ska1ΔMTBD</sup> and Taxol-stabilized microtubules	Ska1ΔMTBD, Ska2, Ska3	Fig. S5
<b>TIRF microscopy experiments</b>		
Ska complex <sup>Ska3-GFP</sup>	Ska1, Ska2, Ska3-GFP	Fig. 1 and Fig. S1
<b>SEC-MALS experiments</b>		
Ska complex <sup>Ska3-GFP</sup>	Ska1, Ska2, Ska3-GFP	Fig. S1

\*All Ska3 proteins were expressed as GST-Ska3 and the GST was removed with TEV cleavage during purification.